Desalination and Water Treatment
www.deswater.com

doi: 10.5004/dwt.2022.28738

271 (2022) 16–26
September

Corrosion inhibition of iron pipes in drinking water distribution systems by a nitrate-reducing bacterium with varied nitrate concentrations

Hui Zhang[a,*], Shasha Liu[a], Shan Chang[b], Yuekai Liu[a]

[a]*School of Environmental and Municipal Engineering, Xi'an University of Architecture and Technology, Xi'an, Shaanxi, China, Tel. +86 02982202729; emails: aoyun9@126.com (H. Zhang), 1210776717@qq.com (S. Liu), 545037988@qq.com (Y. Liu)*
[b]*Zhejiang Province Institute of Architectural Design and Research, Hangzhou, Zhejiang, China, email: 545388275@qq.com (S. Chang)*

Received 22 January 2022; Accepted 23 July 2022

ABSTRACT

Iron pipe corrosion is the main reason of secondary pollution of drinking water, and nitrate-reducing bacteria (NRB) are considered as corrosion-related bacteria. However, the corrosion inhibition effects of NRB are not well publicized, and the inhibition mechanisms have not been well-understood. In this study, the corrosion inhibition of NRB (*Pseudomonas monteilii* CS01, a common nitrate-reducing bacterium) under drinking water conditions was investigated with varied nitrate supplements. Bench-scale reactors were employed to study the iron and nitrate transformation induced by NRB CS01. Four experimental groups were designed under different conditions. The characteristics of corrosion products and corrosion process were determined by physico-chemical analysis and weight loss method, respectively. The iron corrosion/release inhibition induced by CS01 was enhanced with the increase of initial nitrate levels. With NRB CS01 and 20.00 mg/L NO_3^-–N, the corrosion rate and concentrations of total iron and Fe^{2+} were the lowest, with values of 0.036 ± 0.003 mm/y (at 170 d), 2.30 ± 1.25 mg/L and 0.19 ± 0.15 mg/L, respectively. Moreover, the consumption of nitrate and the production of nitrite and ammonium were the highest under this condition. This study may be beneficial for developing the potential strategies for improving drinking water quality and water supply safety.

Keywords: Iron corrosion; Nitrate; Nitrate-reducing bacteria; Iron release; Water distribution system

1. Introduction

Drinking water distribution systems (DWDSs) are essential infrastructure used to transport drinking water to users' taps. During the process, a series of complex physical, chemical or biological reactions occur, resulting in water quality problems, such as elevated turbidity and iron level, reduced disinfectant residual, and bacteria regrowth [1–4]. Iron pipe corrosion is considered to be the main reason of secondary pollution of drinking water, and becomes the most common problem in drinking water distribution [5–9].

Microbiologically influenced corrosion (MIC) refers to the corrosion caused by the activities of microorganisms, playing an important role in iron pipe corrosion in DWDSs [10]. The related bacteria include sulfur-oxidizing bacteria (SOB), sulfate-reducing bacteria (SRB), iron-oxidizing bacteria (IOB), iron-reducing bacteria (IRB), and nitrate-reducing bacteria (NRB). SOB, SRB, and IOB can accelerate corrosion [11,12], while IRB have both promotion and inhibition effects [13]. NRB have been reported to possess corrosive properties, and better understanding of their corrosion mechanism has been obtained in recent

* Corresponding author.

years. A theory known as biocatalytic cathodic nitrate reduction (BCNR) can explain the MIC induced by NRB [14–16]. According to the BCNR theory, nitrate or nitrite can be reduced to NH_4^+ and N_2 for their metabolism, and iron oxidation occurs simultaneously.

Since NRB are usually studied as corrosive microbes, their corrosion inhibition effects have been ignored and there are only a few reports available on this subject. Some researchers proposed that NRB competitively suppressed the growth of SRB and caused the decrease of metal corrosion rate in oil and gas reservoirs suffering from high SRB cell counts [17–19]. Moreover, NRB *Azospira* and *Dechloromonas* were found to oxidate and reduce iron simultaneously when nitrate concentrations were lower than 0.5 mM, resulting in corrosion inhibition [20–22]. Wang et al. [23] pointed that NRB *Dechloromonas hortensis* could promote or reduce iron corrosion under different nitrate concentrations. Therefore, the corrosion inhibition mechanisms of NRB have not been well-understood.

Recently, our research indicated that nitrate addition could promote the growth of NRB in DWDSs, causing the constant decrease of iron corrosion/release in cast iron pipes [24]. However, there was little change of SRB relative abundance with the increase of nitrate concentrations. Thus, the competition of NRB against SRB cannot explain the inhibition effect. To investigate the corrosion inhibition by NRB in our research, a nitrate-reducing bacterium, *Pseudomonas monteilii* CS01, was isolated from the experimental pipes. *Pseudomonas* sp. have been identified as heterotrophic nitrate reducers with corrosive properties [25,26]. However, their corrosion inhibition properties are not widely known. Additionally, the role and effects of NRB in real DWDSs (aerobic and oligotrophic environments) during the pipe corrosion processes are still poorly understood.

Consequently, in this study, the inhibition effects of NRB on iron pipe corrosion in DWDSs under varied nitration concentrations (≤20.00 mg/L, the acceptable level of nitrate in drinking water in China) were investigated. *P. monteilii* CS01, isolated previously, was used as a common nitrate-reducing bacterium, and most *Pseudomonas* sp. are facultative which means they can respire oxygen. The characteristics of corrosion products and corrosion process were determined by physico-chemical analysis and weight loss method, respectively. Bench-scale reactors were employed to study the iron and nitrate transformation induced by NRB CS01. The findings may be of significant relevance in the maintenance of iron pipe infrastructures and water supply safety.

2. Materials and methods

2.1. Bacteria preparation and culture medium

NRB CS01 was isolated previously from the corrosion scales of cast iron pipes in the DWDSs Xi'an, China. It was preserved in the lab (20% glycerol at –80°C), and obtained for reviving on Trypticase Soy Agar (TSA) medium under oxic conditions. The medium contained (per liter of distilled water) 15.0 g tryptone, 5.0 g soy peptone and 5.0 g NaCl, and pH was adjusted at 7.3 ± 0.2. The medium was autoclaved for sterilization (121°C for 30 min).

TSA medium was inoculated by colonies of this culture and incubated under orbital agitation (30°C and 150 rpm). After 24 h, the cells were harvested and centrifuged (8,000 g at 4°C for 10 min), and then washed twice and re-suspended in 9% NaCl to obtain a final cell density of 4.60 ± 0.25 × 10^9 cells/mL. The glassware used in the experiment were all autoclaved (121°C for 30 min), and the experiment was performed in a sterile environment to prevent contamination.

2.2. Experimental water quality

The experimental water used in this study was tap water, which was distributed by Xi'an DWDSs and treated by chemical flocculation, settling, sand filtration, and disinfection by chlorine. The tap water was autoclaved for the sterile water (121°C for 30 min). Table 1 shows the values of water quality parameters, which were measured based on the standard methods of water and wastewater examinations [27]. Dissolved oxygen (DO), pH, oxidation–reduction potential (ORP) and conductivity were determined using a HACH HQ30D multimeter. The concentrations of total iron and Fe^{2+} were measured according to the 1,10-phenanthroline method [28]. The levels of NO_3^-–N, NO_2^-–N and NH_4^+–N were measured colorimetrically [20,21].

2.3. Experiment design of corrosion on cast iron coupons

In this study, cast iron coupons (27 mm × 55 mm × 5 mm, Dongguan RISHUN Metals Materials Co., Ltd., Dongguan, China) were used for the corrosion experiments. The elemental composition (wt.%) of the coupons was C 3.58%, Si 2.26%, Mn 0.81%, P 0.086%, S 0.032%, and Fe 93.232%. Before the experiments, the cast iron coupons were sequentially ground with silicon carbide sandpapers (180, 500, 800, and 1,200 grit). Then, a series of treatments were performed on the ground coupons, including rinsing with sterile deionized water three times, degreasing in acetone, sterilizing by 70% (v/v) ethanol for 8 h, and drying in an

Table 1
Tap water quality and sterile water quality in the experiment

Parameter (Unit)	Tap water	Sterile water
pH	7.34–8.38	7.34–8.38
DO (mg/L)	7.00–9.70	3.97–7.11
Conductivity (μS/cm)	70–270	72.5–259
ORP (mV)	140–400	85.7–265.4
Alkalinity (mg $CaCO_3$/L)	70–74	64.92–68.50
Cl^- (mg/L)	10–24	9.32–10.45
SO_4^{2-} (mg/L)	15–30	13.89–15.01
Total iron (mg/L)	0.02–0.28	0.05–0.06
Fe^{2+} (mg/L)	0–0.005	0–0.005
NO_3^-–N (mg/L)	1.41–2.95	1.66–3.09
NO_2^-–N (mg/L)	0–0.004	0.001–0.005
NH_4^+–N (mg/L)	0.059–0.118	0.067–0.119

oven. Finally, the coupons were exposed to UV light for 30 min, weighted, and marked for further use.

All reagent solutions were autoclaved for sterilization before use. Four experimental groups were designed under different conditions. For one group, two cast iron coupons were immersed in the sterile water in a 500 mL bottle sealed up with a plastic film. For the other three groups, CS01 was added, and sodium nitrate solution was used for two groups to adjust the initial nitrate concentrations to 10.00 and 20.00 mg/L. The water was replaced every 48 h to reflect the maximum hydraulic residence time and the worst situation in actual DWDSs [29,30]. Each bottle was placed on a magnetic agitator to simulate the water flow in actual DWDSs. Water samples were also collected every 48 h to determine the concentrations of NO_3^-–N, NO_2^-–N, NH_4^+–N, total iron and Fe^{2+}.

The experiment was repeated three times, and the average values were shown in figures and tables. SPSS 22.0 (SPSS Inc., USA) was used for statistical analysis, and p-value < 0.05 was considered statistically significant.

2.4. Corrosion products characterization and corrosion rate calculation

To characterize the corrosion products and calculate the corrosion rate, another four experimental groups were performed under the designed conditions. For each group, two cast iron coupons were sampled at different durations (20, 60, 90, and 170 d). The water in each bottle was replaced every 2 d. The coupons were employed for vacuum freeze-drying, and then scraped gently to collect corrosion products with a sterilized blade. The surface features, crystalline phase, and elemental composition of the corrosion products were examined using scanning electron microscopy (SEM, Sigma HD, Zeiss, Germany), X-ray diffraction (XRD, Ultima IV, Rigaku, Japan) and X-ray fluorescence (XRF, ZSX Primus, Rigaku, Japan), respectively.

The scraped coupons were cleaned using cotton swabs and 70% (v/v) ethanol, promptly freeze-dried, and weighed to determine the corrosion rate [23]. The following equation based on the weight loss method can be used for calculating the corrosion rate [31].

$$v_{corr} = \frac{8.76 \times 10^4 \times \left(w_0 - w_1\right)}{\rho \times A \times t} \quad (1)$$

where v_{corr} is the corrosion rate (mm/a); w_0 and w_1 are the original and final weights (g), respectively; ρ is the coupon density (g/cm^3); A is the exposed coupon area (cm^2); and t is the corrosion time (h).

3. Results and discussion

3.1. Characteristics of corrosion products

To reveal the microstructure of the corrosion products on cast iron coupons, some representative SEM images at 170 d under different conditions are shown in Fig. 1. In the

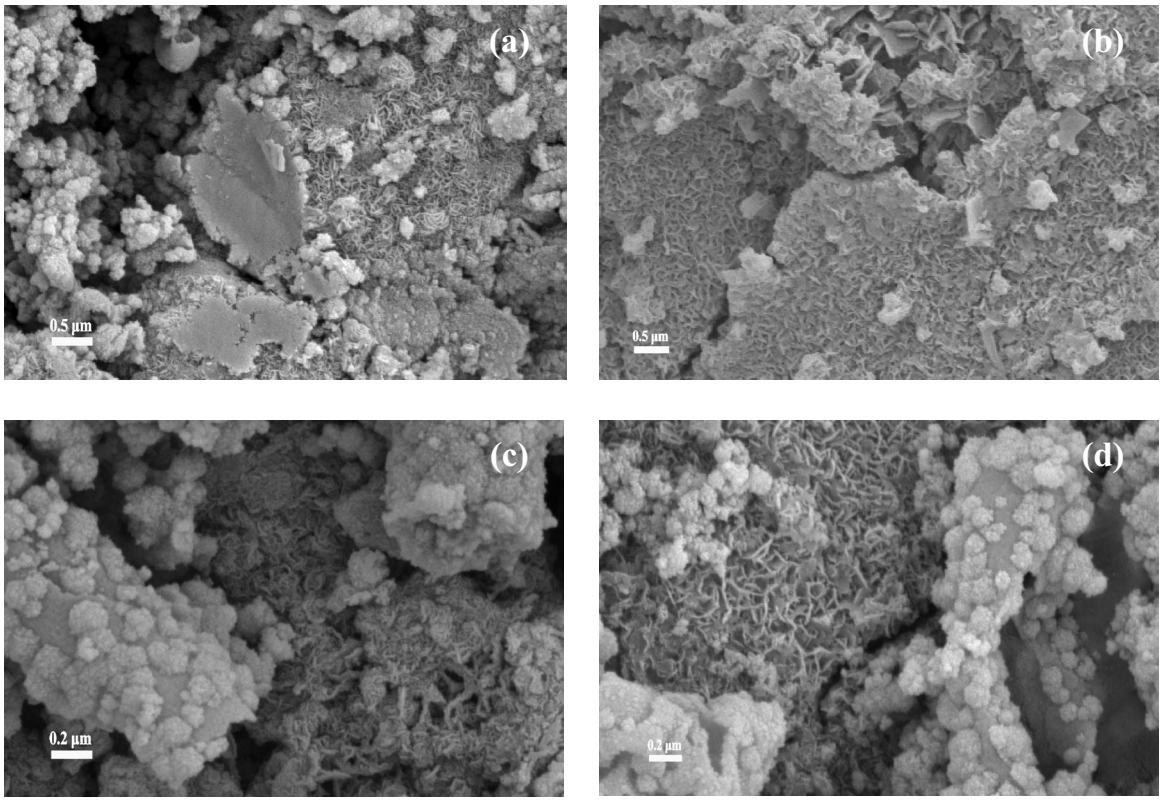

Fig. 1. SEM images of corrosion products on iron cast coupons at 170 d. (a) Sterile water, (b) sterile water with CS01, (c) CS01 with 10.00 mg/L NO_3^-–N, and (d) CS01 with 20.00 mg/L NO_3^-–N.

sterile water, acicular minerals and granular crystal structures were found in the corrosion products (shown in Fig. 1a), and they were considered to be goethite (α-FeOOH) and calcite ($CaCO_3$), respectively. With NRB CS01, some different morphologies were observed. Besides the acicular minerals, leaf-like and lamellar minerals were found in Fig. 1b and c, respectively, and they were also considered as α-FeOOH. When the initial nitrate concentration was increased to 20.00 mg/L, stacked spherical minerals, regarded as magnetite (Fe_3O_4), appeared in the corrosion products (shown in Fig. 1d).

Fig. 2 shows the crystalline compounds of the corrosion products under different conditions at 170 d. Under the four experimental conditions, α-FeOOH, $CaCO_3$ and Fe_3O_4 were found in the corrosion products. Although Fe_3O_4 was observed in all samples, its intensity of XRD peaks under the condition of CS01 with 20.00 mg/L NO_3^-–N was higher than that under any other condition. Thus, the formation of Fe_3O_4 might be promoted by CS01 with increased initial NO_3^-–N concentrations. Since Fe_3O_4 is thermodynamically stable and usually possesses protective and anti-corrosive properties, further corrosion may be inhibited by CS01 with higher NO_3^-–N levels [32,33]. This was confirmed by the corresponding SEM images.

The peak intensity of $CaCO_3$ was found in the sterile water, whereas in the samples with NRB CS01, it disappeared, and siderite ($FeCO_3$) was detected. Therefore, CS01 could affect the crystalline composition and conversion of corrosion products by inducing iron oxidation/reduction, which was in accordance with the previous study by Pillay and Lin [34].

The elemental compositions of different corrosion products were determined using XRF analysis, and the results are shown in Table 2. The corrosion products under any condition consisted mostly of metal elements. In the sterile water, the primary elements were iron (Fe) (85.48%) and calcium (Ca) (9.26%), indicating that the concentrations of total Fe and Ca accounted for 0.855 and 0.093 g/g, respectively. The high Fe concentration originated from the cast iron coupons, whereas Ca primarily originated from the experimental water and formed calcite deposit. The other elements including silicon (Si), manganese (Mn), titanium (Ti), magnesium (Mg), chromium (Cr), aluminum (Al), nickel (Ni), vanadium (V), copper (Cu), and zinc (Zn) were in the order of decreasing prevalence. The contents of Si, Mn, Ti, Mg and Cr were higher than 0.10%, while those of Al, Ni, V, Cu and Zn were less than 0.10%. This finding was similar to the previous study, which indicated that the trace inorganic contaminants V, Ni, Cu, Al, and Zn were at extremely low levels in corrosion scales in DWDSs [35]. The accumulation of some elements (Si, Mn, Ti, Mg and Cr) in this study was related to the water quality and absence of microorganism.

With CS01, the percentages of total Fe in corrosion products were higher than 94.50%, while that of Ca were reduced to less than 1.00%. The total percentages of other elements under the three conditions of CS01 with sterile water, 10.00 and 20.00 mg/L NO_3^-–N were also decreased

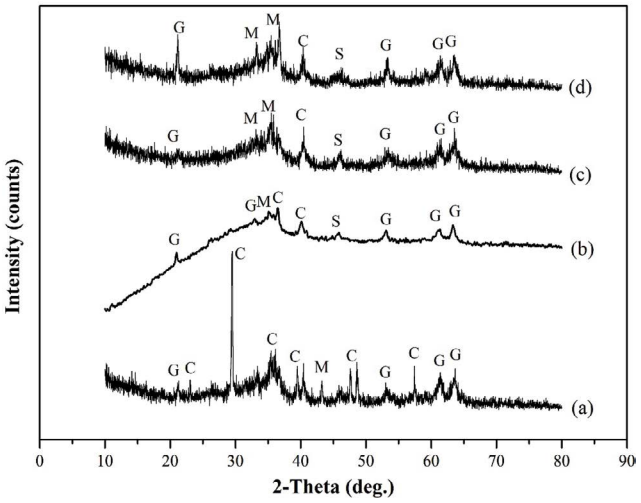

Fig. 2. XRD patterns of the corrosion products on cast iron coupons at 170 d. (a) Sterile water, (b) sterile water with CS01, (c) CS01 with 10.00 mg/L NO_3^-–N, and (d) CS01 with 20.00 mg/L NO_3^-–N. (G-goethite, M-magnetite, C-calcite, S-siderite).

Table 2
Elemental compositions of different corrosion products on cast iron coupons by XRF (%)

Elements	Sterile water	CS01 + sterile water	CS01 + 10.00 mg/L NO_3^-–N	CS01 + 20.00 mg/L NO_3^-–N
Iron (Fe)	85.48	94.60	94.60	94.66
Calcium (Ca)	9.26	0.62	0.49	0.41
Silicon (Si)	3.69	3.64	3.68	3.71
Manganese (Mn)	0.76	0.40	0.43	0.41
Titanium (Ti)	0.18	0.11	0.09	0.12
Magnesium (Mg)	0.17	0.05	0.05	0.05
Chromium (Cr)	0.10	0.05	0.04	0.06
Aluminum (Al)	0.05	0.05	0.06	0.06
Nickel (Ni)	0.04	0.02	0.03	0.03
Vanadium (V)	0.03	0.02	0.01	0.02
Copper (Cu)	0.02	0.01	0.01	0.01
Zinc (Zn)	0.02	0.02	0.02	0.01

to 4.37%, 4.42%, and 4.48%, respectively. Accordingly, the NRB could make contributions to iron redox behavior, resulting in the composition transformation of corrosion products. With the increase of the initial NO_3^-–N concentrations in water, the concentrations of Ca were decreased to some extent. The main reason may be that $FeCO_3$ with much lower solubility than $CaCO_3$ was generated with the presence of CS01 (shown in Fig. 2). NRB CS01 with higher initial NO_3^-–N levels may increase the amounts of $FeCO_3$ precipitation. Moreover, the fractions of other elements (Si, Mn, Ti, Mg, Cr, Al, Ni, V, Cu and Zn) went up slightly as the initial NO_3^-–N concentrations increased. That may be due to the combination of surface adsorption by the corrosion products, extracellular polymer substances (EPS) and biofilms on the cast iron coupons [36,37].

3.2. Variations of total iron and Fe^{2+} concentrations

Figs. 3 and S1 show the variations of total iron concentrations under different conditions. During the experiment, most values of total iron concentrations were highest in the sterile water and lowest with CS01 and 20.00 mg/L NO_3^-–N. Furthermore, under each condition, the total iron levels were gradually increased to the maximum during the first 40 days and then showed a sawtooth pattern, decreasing to relatively stable values. The highest values under the sterile water, CS01 with sterile water, CS01 with 10.00 mg/L NO_3^-–N, and CS01 with 20.00 mg/L NO_3^-–N were 9.21 mg/L (at 40 d), 7.89 mg/L (at 40 d), 5.56 mg/L (at 40 d), and 4.88 mg/L (at 22 d), respectively. Additionally, the average total iron concentrations under the four conditions were 5.63 ± 1.88 mg/L, 3.77 ± 1.73 mg/L, 2.86 ± 1.41 mg/L, and 2.30 ± 1.25 mg/L, respectively. The mean value of total iron in the sterile water was significantly higher than those under other conditions ($p = 0.000 < 0.001$).

After adding CS01, the average total iron concentrations with 10.00 mg/L ($p = 0.004 < 0.01$) and 20.00 mg/L NO_3^-–N ($p = 0.000 < 0.001$) were significantly reduced. However, the mean values of total iron concentrations showed no significant difference between CS01 with 10.00 and 20.00 mg/L NO_3^-–N. It was clear that the total iron levels could be greatly decreased by the NRB and initial NO_3^-–N concentrations.

The changes of Fe^{2+} concentrations in the experiment are described in Figs. 4 and S2 for comparison. Most Fe^{2+} concentrations in the sterile water were the highest whereas those with CS01 and 20.00 mg/L NO_3^-–N were the lowest. This was consistent with the variations of total iron concentrations. In the sterile water, Fe^{2+} concentrations went up to 1.00 mg/L at 46 d, and then were decreased gradually with some fluctuations. With CS01, all maximum values of Fe^{2+} concentrations (0.71, 0.66, and 0.65 mg/L) were recorded at 34 d, which was earlier than the duration of the highest Fe^{2+} level in the sterile water. After 42 d, Fe^{2+} concentrations with the NRB were reduced to relatively stable values. The average values of Fe^{2+} concentrations under the four conditions were 0.44 ± 0.24 mg/L, 0.29 ± 0.19 mg/L, 0.23 ± 0.17 mg/L, and 0.19 ± 0.15 mg/L, respectively. Similarly, the mean Fe^{2+} concentration in the sterile water was significantly higher than that under the other three conditions ($p = 0.000 < 0.001$), and the average values showed no significant difference between CS01 with 10.00 and 20.00 mg/L NO_3^-–N.

Figs. 3 and 4 clearly show that under each condition, only a small part of iron released in water was soluble Fe^{2+}. The ratios of Fe^{2+} to total iron concentrations during the experiment are illustrated in Table 3. In the sterile water, the portion of Fe^{2+} concentrations varied from 0.017 to 0.097, with an average of 0.063 ± 0.019, implying that means under this condition, more than 90% of the released iron was in the form of ferric iron (Fe(III)), which was consistent with the findings of other studies [24,38]. With the NRB, the ratios changed in wider ranges, which were 0.013–0.156, 0.013–0.248, and 0.017–0.217 under the three conditions of CS01 with sterile water, 10.00 and 20.00 mg/L NO_3^-–N, respectively. The main reason may be that NRB CS01 could influence the transformation between Fe(II) and Fe(III), resulting in notable variations of the total iron and Fe^{2+} contents.

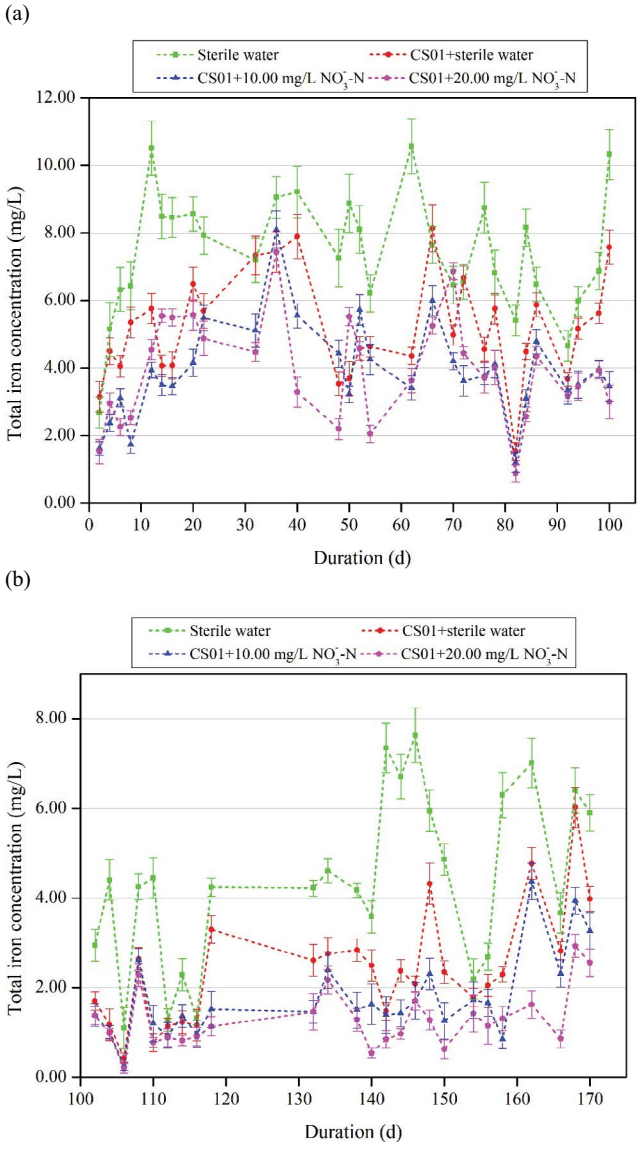

Fig. 3. Variations of total iron concentrations during the experiment: (a) From 0 to 100 d and (b) from 100 to 170 d.

3.3. Nitrogen transformation under different conditions

Figs. 5–7 and S3–S5 illustrate the changes of nitrate consumption and nitrite and ammonium production. The consumption of NO_3^-–N in the sterile water varied in the range of 0.42–2.05 mg/L, with an average of 1.31 ± 0.31 mg/L, which was significantly lower than the means of NO_3^-–N consumption with CS01 ($p < 0.01$). Without the NRB, the average amounts of NO_2^-–N and NH_4^+–N production were 0.007 ± 0.013 mg/L and 0.81 ± 0.43 mg/L, respectively, revealing significant differences with respect to those under other conditions ($p < 0.001$). Accordingly, nitrogen transformation occurred under this condition, and approximately 0.53% and 61.83% of decreased NO_3^-–N were converted to NO_2^-–N and NH_4^+–N, respectively.

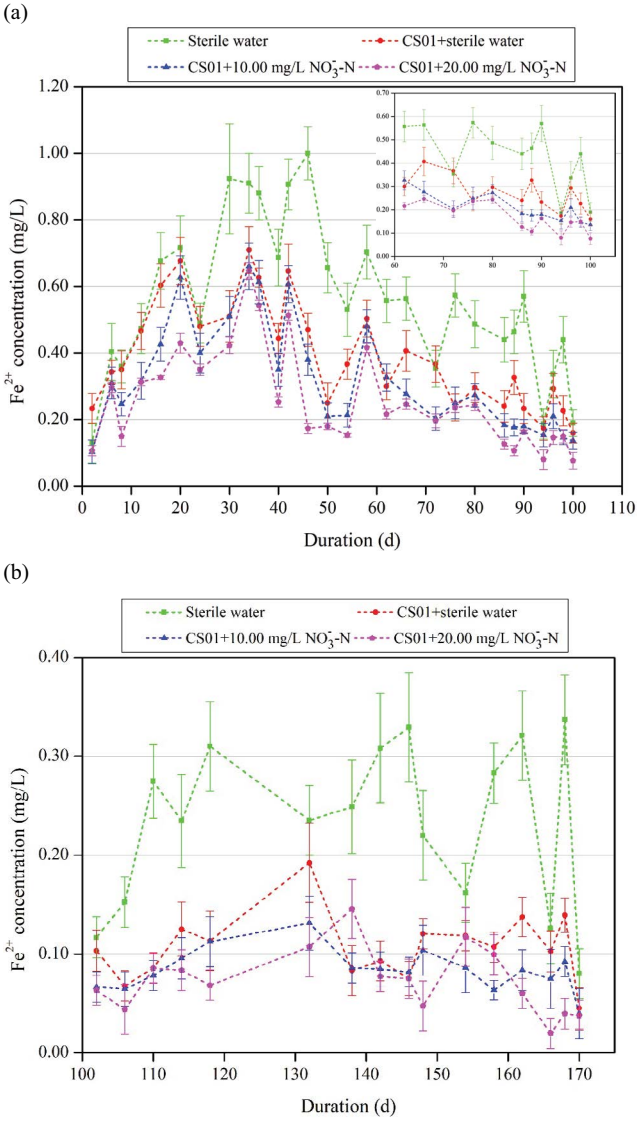

Fig. 4. Variations of Fe^{2+} concentrations during the experiment: (a) From 0 to 100 d and (b) from 100 to 170 d.

Compared with the sterile water, the ranges of NO_3^-–N consumption under the other three conditions of CS01 with sterile water, 10.00 and 20.00 mg/L NO_3^-–N were 1.14–2.50 mg/L, 2.21–5.82 mg/L, 1.75–6.54 mg/L, respectively. The means of NO_3^-–N consumption under the three conditions were 1.80 ± 0.40 mg/L, 3.79 ± 0.97 mg/L, and 4.62 ± 1.19 mg/L, respectively. With the same initial nitrate levels, the average content of consumed NO_3^-–N with CS01 was increased gradually. Therefore, the respiration of the NRB could promote the consumption of NO_3^-–N, and the promotion also took place under higher initial NO_3^-–N levels. A significant difference was recorded in the average amounts of consumed NO_3^-–N between any two conditions ($p < 0.01$).

The means of produced NO_2^-–N with CS01 and sterile water, 10.00 and 20.00 mg/L NO_3^-–N were 0.046 ± 0.034 mg/L, 0.19 ± 0.05 mg/L and 0.24 ± 0.07 mg/L, respectively. The average amounts of NH_4^+–N production were 1.60 ± 0.37 mg/L, 3.42 ± 0.45 mg/L and 3.81 ± 0.45 mg/L under the three conditions. Accordingly, the concentrations of produced NH_4^+–N with the NRB were higher than that in the sterile water. In addition, the amounts of reduced NO_3^-–N and produced NO_2^-–N and NH_4^+–N with the presence of CS01 were higher than that with NRB *D. hortensis* reported by the study of Wang et al. [23]. The differences may be due to the different characteristics of the two bacterial strains. In this experiment, the values of DO varied in the range of 3.97–7.11 mg/L, which constituted an aerobic environment and might be more suitable for the growth of CS01. By increasing the initial concentrations of NO_3^-–N, NRB CS01 could use more NO_3^-–N as nutrients for their growth and reproduction, causing the enhancement of their nitrate reduction.

3.4. Corrosion rate of cast iron coupons

Using Eq. (1), the corrosion rates of cast iron coupons under different conditions were calculated, as illustrated in Fig. 8. Under each condition, the corrosion rate at 60 d

Table 3
Statistics of the ratios of Fe^{2+} to total iron concentrations under different conditions

Experimental condition	Mean	SD	Max.	Min.	95% CI	
					Upper	Lower
Sterile water	0.063	0.019	0.097	0.017	0.069	0.056
CS01 + sterile water	0.065	0.032	0.156	0.013	0.076	0.053
CS01 + 10.00 mg/L NO_3^-–N	0.070	0.043	0.248	0.013	0.085	0.055
CS01 + 20.00 mg/L NO_3^-–N	0.074	0.041	0.217	0.017	0.088	0.059

SD is standard deviation, Max. is maximum, Min. is minimum, and CI is confidence interval.

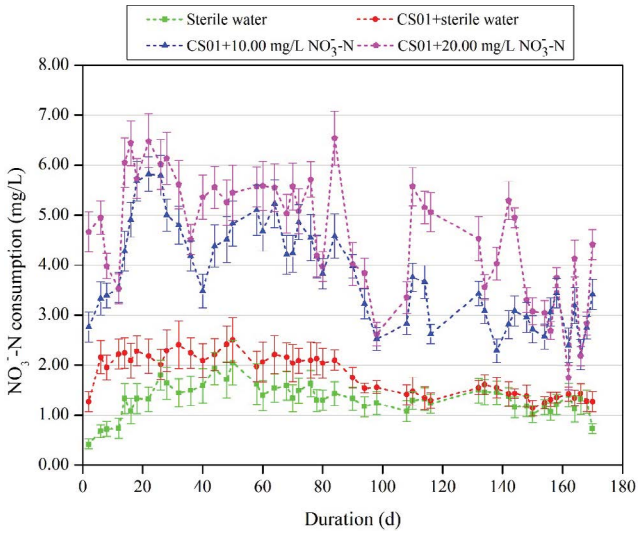

Fig. 5. Amount of NO_3^-–N consumption under different conditions during the experiment.

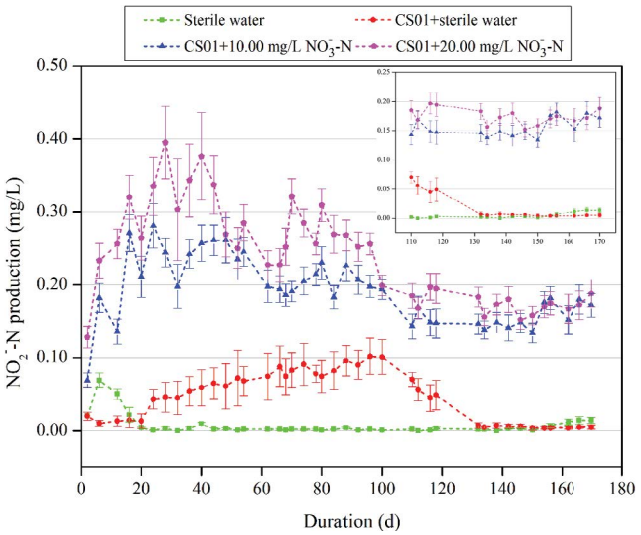

Fig. 6. Amount of NO_2^-–N production under different conditions during the experiment.

was the maximum, while that at 170 d was the minimum. Therefore, the corrosion rates under different conditions all presented the same trend of increasing first and decreasing later. Additionally, the corrosion rates of cast iron coupons in the sterile water were much higher than that with CS01 of the same duration. Without the NRB, the corrosion rates at 20, 60, 90, and 170 d were 0.101 ± 0.027 mm/y, 0.186 ± 0.029 mm/y, 0.078 ± 0.013 mm/y, and 0.054 ± 0.008 mm/y, respectively. However, the corrosion rates under the same initial NO_3^-–N levels with CS01 were reduced significantly: 0.093 ± 0.006 mm/y (at 20 d), 0.096 ± 0.006 mm/y (at 60 d), 0.077 ± 0.011 mm/y (at 90 d), and 0.053 ± 0.004 mm/y (at 170 d). Thus, iron corrosion was inhibited by NRB CS01.

Moreover, the corrosion rates with CS01 were decreased gradually with the increase of initial concentrations of NO_3^-–N. With 10.00 mg/L NO_3^-–N, the corrosion rates at 20, 60, 90, and 170 d were reduced to 0.087 ± 0.004 mm/y, 0.093 ± 0.008 mm/y, 0.071 ± 0.011 mm/y, and 0.047 ± 0.001 mm/y, respectively. When the initial NO_3^-–N concentrations went up to 20.00 mg/L, further decreases of the corrosion rate were recorded, and the values were 0.081 ± 0.007 mm/y at 20 d, 0.083 ± 0.008 mm/y at 60 d, 0.070 ± 0.018 mm/y at 90 d, and 0.036 ± 0.003 mm/y at 170 d. The decreases of the corrosion rates under higher initial NO_3^-–N levels were primarily owing to the formation of NRB biofilm, which was promoted by nitrate and acted as oxygen (O_2) barrier.

3.5. Corrosion inhibition of NRB CS01 with varied NO_3^-–N concentrations

In this study, the corrosion inhibition of NRB CS01 with varied initial nitrate concentrations was investigated. Without CS01, $CaCO_3$ and α-FeOOH were prevalent in the corrosion products. Under this condition, elemental iron was deemed as the electron donor to form Fe^{2+}, while nitrate was reduced to ammonium as the electron acceptor, as described in Eq. (2) [39].

$$4Fe + NO_3^- + 10H^+ \rightarrow 4Fe^{2+} + NH_4^+ + 3H_2O \quad (2)$$

Ferrous iron could be oxidized by DO to form α-FeOOH [displayed in Eq. (3)], which was a component of the corrosion products with a loose and porous morphology. Thus, iron can be easily released into the water, causing the highest concentrations of total iron (mean: 5.63 ± 1.88 mg/L) and Fe^{2+} (mean: 0.44 ± 0.24 mg/L). The corrosion rates at 20, 60, 90, and 170 d were 0.101 ± 0.027 mm/y, 0.186 ± 0.029 mm/y, 0.078 ± 0.013 mm/y, and 0.054 ± 0.008 mm/y, respectively, which were higher than those under other conditions. Moreover, the consumption of NO_3^-–N and production of NO_2^-–N and NH_4^+–N were the lowest. On average, approximately 1.31 ± 0.31 mg/L nitrate was consumed to produce ammonium.

$$2Fe^{2+} + \frac{1}{2}O_2 + 4OH^- \rightarrow 2\alpha - FeOOH + H_2O \quad (3)$$

However, in the water with CS01, obvious changes were monitored during the experiment, including the composition of corrosion products, amount of released iron, corrosion rate, and biologically mediated process of nitrate reduction. First, the intensity of Fe_3O_4 was enhanced with the addition of CS01 and increase of initial NO_3^-–N concentrations. Therefore, NRB CS01 combined with increased nitrate concentrations could affect the composition of corrosion products and promote the formation of Fe_3O_4 [23].

Furthermore, with the addition of CS01, the concentrations of total iron and Fe^{2+} were reduced with the means of 3.77 ± 1.73 mg/L and 0.29 ± 0.19 mg/L, respectively. The corrosion rates were decreased to 0.093 ± 0.006 mm/y (at 20 d), 0.096 ± 0.006 mm/y (at 60 d), 0.077 ± 0.011 mm/y (at 90 d), and 0.053 ± 0.004 mm/y (at 170 d). Thus, iron corrosion/release was inhibited. The inhibition effects were enhanced by the increase of nitrate concentrations. Some NRB have shown to be capable of reducing ferric compounds such as α-FeOOH to produce Fe_3O_4 through respiration [20,23].

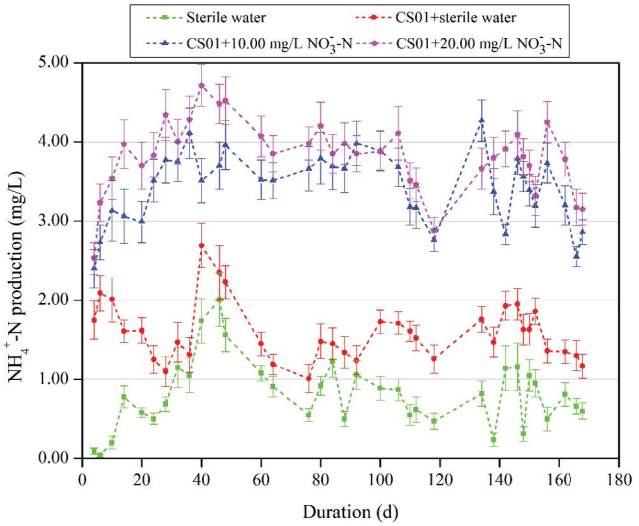

Fig. 7. Amount of NH_4^+–N production under different conditions during the experiment.

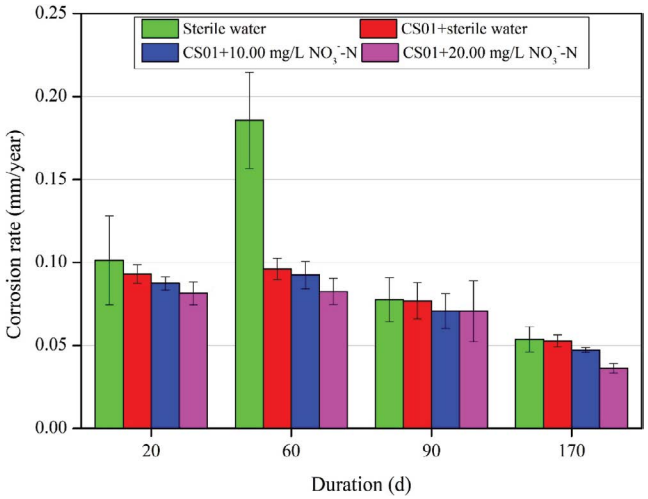

Fig. 8. Corrosion rates of the cast iron coupons under different conditions.

In this study, CS01 with higher nitrate levels may be helpful for the formation of Fe_3O_4, which made the corrosion products become compact and dense. Consequently, the quantities of total iron and Fe^{2+} were reduced. In addition, the NRB biofilm formed on the cast iron coupons, and it can reduce DO underneath the biofilm by acting as a physical barrier. Thus, iron corrosion by oxygen was inhibited, and the inhibition was enhanced by the increase of nitrate levels due to the formation of denser biofilm.

Finally, enhanced nitrate depletion and nitrite and ammonium production were observed in the experiments with CS01, and they were increased concomitantly with the elevated initial nitrate levels. Nitrate reduction proceeded to different extents under the respiration of CS01. The average concentration of nitrite production was only 0.007 ± 0.013 mg/L in the sterile water, whereas it went up to 0.046 ± 0.034 mg/L, 0.19 ± 0.05 mg/L and 0.24 ± 0.07 mg/L under the conditions of CS01 with sterile water, 10.00 and 20.00 mg/L NO_3^-–N. The main reason may be that nitrate was first reduced to nitrite by the respiration of CS01. The produced nitrite may then be converted to nitrous oxide (N_2O) or nitrogen (N_2). During that process, elemental iron served as the electron donor to generate Fe(II), and Fe(III) was reduced by the NRB to form Fe_3O_4. It could be inferred that both Fe(II)/Fe(III) and Fe/N redox cycling occurred with the presence of CS01, which was consistent with the previous study [23].

Compared with the concentration of nitrite produced, produced ammonium concentration was much higher. The average concentrations of NH_4^+–N production were 1.60 ± 0.37 mg/L, 3.42 ± 0.45 mg/L, and 3.81 ± 0.45 mg/L under the three conditions with NRB CS01. The increase of ammonium production may be the result of nitrate conversion in electrochemical corrosion and some dead cells of the NRB.

In general, NRB CS01 and increased nitrate concentrations could affect the redox of iron and reduction of nitrate, leading to the transformation of corrosion products and inhibition of iron release. Moreover, with the formation of NRB biofilm as O_2 barrier, iron corrosion was inhibited. Nevertheless, *P. monteilii* is facultative, and a facultative NRB biofilm may sustain itself with O_2 respiration if nitrate is lacking in the liquid phase or in the middle of the biofilm. This will impact the NRB's O_2 barrier effectiveness. Therefore, more efforts should be made to explore O_2 diffusion in *P. monteilii* biofilm for deep understanding of the inhibition mechanisms.

4. Conclusions

With NRB CS01 and elevated initial nitrate concentrations, the intensity of Fe_3O_4 in XRD analysis was enhanced. Under the condition of CS01 and 20.00 mg/L NO_3^-–N, the corrosion rates and concentrations of total iron and Fe^{2+} were the lowest, with values of 0.036 ± 0.003 mm/year (at 170 d), 2.30 ± 1.25 mg/L and 0.19 ± 0.15 mg/L, respectively. Moreover, the consumption of nitrate and production of nitrite and ammonium were the highest under this condition. NRB CS01 and increased NO_3^-–N levels could affect the composition of corrosion products, iron redox, and nitrate reduction, and inhibit iron corrosion by the biofilm acting as O_2 barrier. More efforts should be made to understand the corrosion inhibition mechanisms of NRB biofilm for water supply safety.

Acknowledgment

This research was financially supported by the Key Project of Shaanxi Natural Science Basic Research Program (No. 2021JZ-50), the Project of Youth Innovation Team Construction (No. 21JP065), the Grant from Youth Innovation Team of Shaanxi Universities in 2020 (PI: Dr. Haihan Zhang), the Project of Shaanxi Federation of Social Sciences (No. 20CZ-39).

References

[1] X. Cheng, E. Peterkin, G.A. Burlingame, A study on volatile organic sulfide causes of odors at Philadelphia's Northeast Water Pollution Control Plant, Water Res., 39 (2005) 3781–3790.

[2] H. Tong, P. Zhao, H. Zhang, Y. Tian, X. Chen, W. Zhao, M. Li, Identification and characterization of steady and occluded water in drinking water distribution systems, Chemosphere, 119 (2015) 1141–1147.
[3] Y. Wang, G. Zhu, Evaluating the corrosiveness in drinking water distribution system in Yancheng City, China, Desal. Water Treat., 242 (2021) 250–259.
[4] J. Zywiec, B. Tchórzewska-Cieslak, D. Papciak, A. Domon, Changes of microbiological parameters of water in domestic distribution system in terms of water supply safety, Desal. Water Treat., 226 (2021) 37–51.
[5] T.L. Gerke, J.B. Maynard, M.R. Schock, D.L. Lytle, Physiochemical characterization of five iron tubercles from a single drinking water distribution system: possible new insights on their formation and growth, Corros. Sci., 50 (2008) 2030–2039.
[6] P.S. Husband, J.B. Boxall, Asset deterioration and discolouration in water distribution systems, Water Res., 45 (2011) 113–124.
[7] X. Li, H. Wang, C. Hu, M. Yang, H. Hu, J. Niu, Characteristics of biofilms and iron corrosion scales with ground and surface waters in drinking water distribution systems, Corros. Sci., 90 (2015) 331–339.
[8] A. Mesdaghinia, R.N. Nabizadeh, S. Nasseri, S.A. Imran, M.T. Samadi, M. Hadi, Potential for iron release in drinking water distribution system: a case study of Hamedan city, Iran, Desal. Water Treat., 57 (2016) 14461–14472.
[9] H. Tong, P. Zhao, C. Huang, H. Zhang, Y. Tian, Z. Li, Development of iron release, turbidity, and dissolved silica integrated models for desalinated water in drinking water distribution systems, Desal. Water Treat., 57 (2016) 398–507.
[10] H. Zhong, Z. Shi, G. Jiang, Z. Yuan, Decreasing microbially influenced metal corrosion using free nitrous acid in a simulated water injection system, Water Res., 172 (2020) 115470, doi: 10.1016/j.watres.2020.115470.
[11] J. Jin, G. Wu, Y. Guan, Effect of bacterial communities on the formation of cast iron corrosion tubercles in reclaimed water, Water Res., 71 (2015) 207–218.
[12] H. Liu, T. Gu, G. Zhang, W. Wang, S. Dong, Y. Cheng, H. Liu, Corrosion inhibition of carbon steel in CO_2-containing oilfield produced water in the presence of iron-oxidizing bacteria and inhibitors, Corros. Sci., 105 (2016) 149–160.
[13] F. Yang, B. Shi, J. Gu, D. Wang, M. Yang, Morphological and physicochemical characteristics of iron corrosion scales formed under different water source histories in a drinking water distribution system, Water Res., 46 (2012) 5423–5433.
[14] D. Xu, T. Gu, Carbon source starvation triggered more aggressive corrosion against carbon steel by the *Desulfovibrio vulgaris* biofilm, Int. Biodeterior. Biodegrad., 91 (2014) 74–81.
[15] B. Liu, Z. Li, X. Yang, C. Du, X. Li, Microbiologically influenced corrosion of X80 pipeline steel by nitrate reducing bacteria in artificial Beijing soil, Bioelectrochemistry, 135 (2020) 107551, doi: 10.1016/j.bioelechem.2020.107551.
[16] H. Wan, D. Song, D. Zhang, C. Du, D. Xu, Z. Liu, D. Ding, X. Li, Corrosion effect of *Bacillus cereus* on X80 pipeline steel in a Beijing soil environment, Bioelectrochemistry, 121 (2018) 18–26.
[17] K. Alasvand Zarasvand, V.R. Rai, Microorganisms: induction and inhibition of corrosion in metals, Int. Biodeterior. Biodegrad., 87 (2014) 66–74.
[18] C.L. Rempel, R.W. Evitts, M. Nemati, Dynamics of corrosion rates associated with nitrite or nitrate mediated control of souring under biological conditions simulating an oil reservoir, J. Ind. Microbiol. Biotechnol., 33 (2006) 878–886.
[19] L.M. Gieg, T.R. Jack, J.M. Foght, Biological souring and mitigation in oil reservoirs, Appl. Microbiol. Biotechnol., 92 (2011) 263–282.
[20] K.A. Weber, M.M. Urrutia, P.F. Churchill, R.K. Kukkadapu, E.E. Roden, Anaerobic redox cycling of iron by freshwater sediment microorganisms, Environ. Microbiol., 8 (2006) 100–113.
[21] A.J. Coby, F. Picardal, E. Shelobolina, H. Xu, E.E. Roden, Repeated anaerobic microbial redox cycling of iron, Appl. Environ. Microbiol., 77 (2011) 6036, doi: 10.1128/AEM.00276-11.
[22] H. Wang, C. Hu, L. Zhang, X. Li, Y. Zhang, M. Yang, Effects of microbial redox cycling of iron on cast iron pipe corrosion in drinking water distribution systems, Water Res., 65 (2014) 362–370.
[23] H. Wang, C. Hu, L. Han, M. Yang, Effects of microbial cycling of Fe(II)/Fe(III) and Fe/N on cast iron corrosion in simulated drinking water distribution systems, Corros. Sci., 100 (2015) 599–606.
[24] H. Zhang, Y. Liu, L. Wang, S. Liu, Iron release and characteristics of corrosion scales and bacterial communities in drinking water supply pipes of different materials with varied nitrate concentrations, Chemosphere, 301 (2022) 134652, doi: 10.1016/j.chemosphere.2022.134652.
[25] R. Kumaraswamy, S. Ebert, M.R. Gray, P.M. Fedorak, J.M. Foght, Molecular- and cultivation-based analyses of microbial communities in oil field water and in microcosms amended with nitrate to control H_2S production, Appl. Microbiol. Biotechnol., 89 (2011) 2027–2038.
[26] Q. Ma, Y. Cai, Z. He, Complete genome sequence of a novel aerobic denitrifying strain, *Pseudomonas monteilii* CY06, Mar. Geonomics, 47 (2019) 100661, doi: 10.1016/j.margen.2019.02.001.
[27] E.W. Rice, L. Bridgewater, Standard Methods for the Examination of Water and Wastewater, APHA/AWWA/WPCF, Washington, D.C., USA, 2012.
[28] M.S. Rahman, G.A. Gagnon, Bench-scale evaluation of drinking water treatment parameters on iron particles and water quality, Water Res., 48 (2014) 137–147.
[29] H. Liu, K.D. Schonberger, C.-Y. Peng, J.F. Ferguson, E. Desormeaux, P. Meyerhofer, H. Luckenbach, G.V. Korshin, Effects of blending of desalinated and conventionally treated surface water on iron corrosion and its release from corroding surfaces and pre-existing scales, Water Res., 47 (2013) 3817–3826.
[30] H. Wang, S. Masters, M.A. Edwards, J.O. Falkinham, A. Pruden, Effect of disinfectant, water age, and pipe materials on bacterial and eukaryotic community structure in drinking water biofilm, Environ. Sci. Technol., 48 (2014) 1426–1435.
[31] Y. Zhu, H. Wang, X. Li, C. Hu, M. Yang, J. Qu, Characterization of biofilm and corrosion of cast iron pipes in drinking water distribution system with UV/Cl_2 disinfection, Water Res., 60 (2014) 174–181.
[32] P. Sarin, V.L. Snoeyink, J. Bebee, K.K. Jim, M.A. Beckett, W.M. Kriven, J.A. Clement, Iron release from corroded iron pipes in drinking water distribution systems: effect of dissolved oxygen, Water Res., 38 (2004) 1259–1269.
[33] H. Sun, B. Shi, F. Yang, D. Wang, Effects of sulfate on heavy metal release from iron corrosion scales in drinking water distribution system, Water Res., 114 (2017) 69–77.
[34] C. Pillay, J. Lin, Metal corrosion by aerobic bacteria isolated from stimulated corrosion systems: effects of additional nitrate sources, Int. Biodeterior. Biodegrad., 83 (2013) 158–165.
[35] C.-Y. Peng, G.V. Korshin, Speciation of trace inorganic contaminants in corrosion scales and deposits formed in drinking water distribution systems, Water Res., 45 (2011) 5553–5563.
[36] S.V. Lalonde, L.A. Amskold, L.A. Warren, K.O. Konhauser, Surface chemical reactivity and metal adsorptive properties of natural cyanobacterial mats from an alkaline hydrothermal spring, Yellowstone National Park, Chem. Geol., 243 (2007) 36–52.
[37] A.P. Hitchcock, J.J. Dynes, J.R. Lawrence, M. Obst, G.D.W. Swerhone, D.R. Korber, G.G. Leppard, Soft X-ray spectromicros copy of nickel sorption in a natural river biofilm, Geobiology, 7 (2009) 432–453.
[38] M. Li, Z. Liu, Y. Chen, Y. Hai, Characteristics of iron corrosion scales and water quality variations in drinking water distribution systems of different pipe materials, Water Res., 106 (2016) 593–603.
[39] B. Zhen, W.J. Zhang, G. Song, Y. Huang, Iron-dependent nitrate reduction by anammox consortia in continuous-flow reactors: a novel prospective scheme for autotrophic nitrogen removal, Sci. Total Environ., 692 (2019) 582–588.

Supplementary information

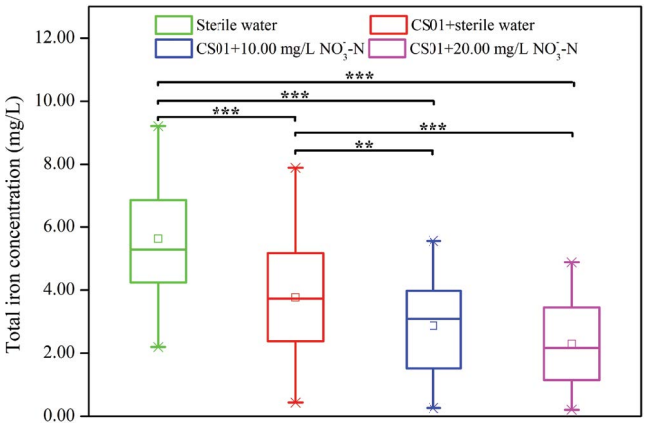

Fig. S1. Variations of total iron concentrations under different conditions. The upper, middle and lower levels of the box represent the 75th, 50th, and 25th percentiles, and the whiskers represent the 95th and 5th percentiles. □ stands for the arithmetic mean and × stands for the maximum and minimum values. The asterisk represents a statistically significant difference between two conditions. * at $p < 0.05$; ** at $p < 0.01$; *** at $p < 0.001$.

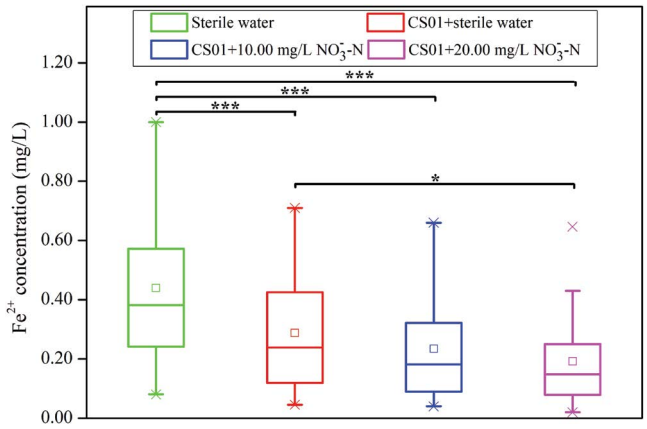

Fig. S2. Variations of Fe^{2+} concentrations under different conditions. The upper, middle and lower levels of the box represent the 75th, 50th, and 25th percentiles, and the whiskers represent the 95th and 5th percentiles. □ stands for the arithmetic mean and × stands for the maximum and minimum values. The asterisk represents a statistically significant difference between two conditions. * at $p < 0.05$; ** at $p < 0.01$; *** at $p < 0.001$.

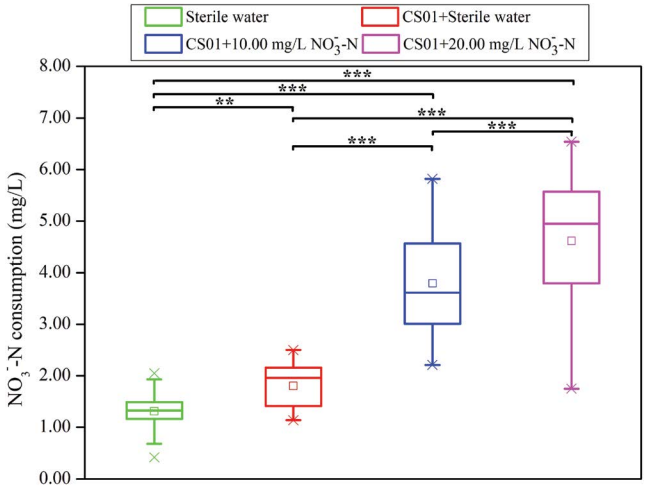

Fig. S3. Variations of NO_3^-–N consumption under different conditions. The upper, middle and lower levels of the box represent the 75th, 50th, and 25th percentiles, and the whiskers represent the 95th and 5th percentiles. □ stands for the arithmetic mean and × stands for the maximum and minimum values. The asterisk represents a statistically significant difference between two conditions. * at $p < 0.05$; ** at $p < 0.01$; *** at $p < 0.001$.

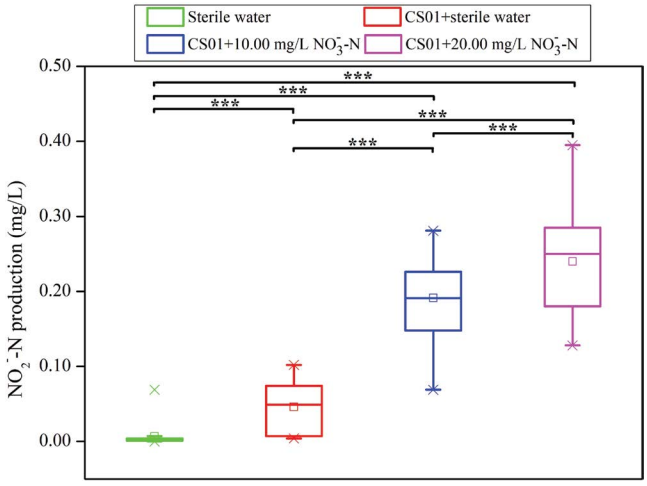

Fig. S4. Variations of NO_2^-–N production under different conditions. The upper, middle and lower levels of the box represent the 75th, 50th, and 25th percentiles, and the whiskers represent the 95th and 5th percentiles. □ stands for the arithmetic mean and × stands for the maximum and minimum values. The asterisk represents a statistically significant difference between two conditions. * at $p < 0.05$; ** at $p < 0.01$; *** at $p < 0.001$.

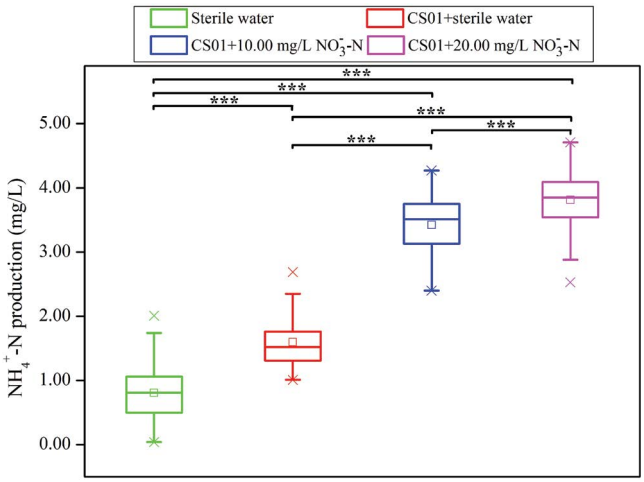

Fig. S5. Variations of NH_4^+–N production under different conditions. The upper, middle and lower levels of the box represent the 75th, 50th, and 25th percentiles, and the whiskers represent the 95th and 5th percentiles. □ stands for the arithmetic mean and × stands for the maximum and minimum values. The asterisk represents a statistically significant difference between two conditions. * at $p < 0.05$; ** at $p < 0.01$; *** at $p < 0.001$.